Engineering and Technology Journal
Journal homepage: https://etj.uotechnology.edu.iq

Analyzing the Impact of FDM Parameters on Compression Strength and Dimensional Accuracy in 3D printed PLA Parts

Hind H. Abdulridha* , **Tahseen F. Abbas**

Production Engineering and Metallurgy Dept., University of Technology-Iraq, Alsina'a street, 10066 Baghdad, Iraq.
*Corresponding author Email: Hind.H.Abdulridha@uotechnology.edu.iq

HIGHLIGHTS

- The impact of infill parameters on compressive strength and the dimensional accuracy deviation of PLA was investigated
- Infill density had the most impact on strength, while layer thickness had the greatest impact on dimensional accuracy.
- The model fits the data well, with a max of 0.44% and 0.948% error for strength and average deviation, respectively.

ARTICLE INFO

Handling editor: Omar Hassoon

Keywords:
Compression strength
Dimensional accuracy
Fused deposition modeling FDM
PLA
Process parameters

ABSTRACT

Fused deposition modeling (FDM) is an additive manufacturing (AM) technique frequently used to create prototypes and parts with intricate geometrical designs. It is gaining popularity since it enhances products by removing the need for expensive equipment. The materials used, the printing process, and the parameters influence the mechanical properties of printed objects. The quality and functionality of the parts are impacted by FDM process parameters. This study focused on the impact of six parameters on the mechanical and physical properties of samples printed using the FDM machine (Creality Ender-5 Pro). The infill density percentage, infill pattern, layer thickness, shell thickness, number of top/bottom layers, and the percentage of infill overlap have been taken as the process parameters. The compressive strength has been calculated using the ASTM D695 compression test. The results illustrated how printing parameters affected samples' mechanical and physical properties, which were proven by the ultimate compression stress UCS and the percentage of compression average deviation. The analysis of variance shows the significance of infill density (100%) for UCS, while layer thickness (0.15 mm) is significant for compression average percentage deviation. For instance, the increase in the infill density from 20% to 100% shows that the strength climbed from 4 MPa to 56.5 MPa. Similarly, reducing layer thickness from 0.3 mm to 0.15 mm results in a diminished dimensional accuracy deviation from 1.65% to 0.446%, approximately three times less than that of the specimen with a 0.3 mm layer thickness.

1. Introduction

Three-dimensional printing technology, called fused deposition modeling (FDM), has created new opportunities for producing parts that would be difficult or impossible to manufacture using conventional methods [1,2]. This technology selectively joins materials layer by layer to build the required component based on a 3D Computer-Aided Design (CAD) model [3]. Non-metallic 3D printing frequently employs materials such as Polylactic Acid (PLA) and Acrylonitrile Butadiene Styrene (ABS) [4]. PLA, in particular, has gained popularity due to its affordability, wide availability, and lightweight properties [5]. Additionally, 3D-printed parts made from PLA tend to exhibit superior mechanical characteristics compared to those made from ABS [6]. In FDM systems, a filament is typically melted and extruded through a nozzle. The extruded polymer is deposited layer by layer on the build plate by moving the nozzle head in three degrees of freedom (DOFs) based on G-code instructions. Continuous filament feed is achieved using two rollers spinning in opposite directions. Consequently, the part's shape and size are gradually constructed by depositing layers of material on the build plate [7]. During the layering process, the printer nozzle follows the spatial coordinates of the CAD model specified in the G-code files to create the part's size and structure. A three-dimensional CAD model is created at the outset of the FDM process. The STL format, commonly used in FDM Cura software, simplifies this model's geometry and transfers it to slicing software. This software segments the part into several fundamental triangular components. Subsequently, the slicing software generates a hardware process plan for the FDM machine using this data [8,9]. Compressive tests based on ASTM D695 have assessed material characteristics based on printing parameters [10].

http://doi.org/10.30684/etj.2023.143615.1599
Received 27 September 2023; Received in revised form 09 November 2023; Accepted 13 November 2023; Available online 11 December 2023
2412-0758/University of Technology-Iraq, Baghdad, Iraq

Numerous works have been performed to optimize the production parameters for the FDM process to produce high-quality printed parts. For instance. Kumar et al. [11] explored the evolution of processing defects and the correlation of mechanical behavior with process parameters in 3D printing. It uses the L27 orthogonal array and Criteria Importance through Intercriteria Correlation (CRITIC) embedded Weighted Aggregated Sum Product Assessment (WASPAS) to optimize parts' mechanical attributes. The study found that layer thickness, print speed, and temperature significantly control part quality and strength. The results showed a maximum flexural strength of 78.52 MPa, an ultimate tensile strength of 45.52 MPa, and an impact strength of 6.21 kJ/m^2. Ambade et al. [12] investigated the effect of infill pattern and density on compressive strength, determining ultimate compressive strength, Young's modulus, and strength-to-weight ratio. Bedan et al. [13] explored the interactive influence of process parameters (infill density and shell thickness) on ABS prints, assessing relative strength, weight, and compressive strength through compression tests. Sivaraos et al. [14] developed an Artificial Neural Network (ANN) model to optimize dimensional properties in 3D printing (FDM) using control factors like layer thickness, orientation, raster angle, raster width, and air gap. The model, with 15 neurons and 2 layers, demonstrated accurate predictions with percentage errors ranging from 0.01% to 25.49% for length, less than 10% for weight, and less than 4% for thickness. This model can be extended to optimize other additive manufacturing process parameters. Farooq et al. [15] examined the impact of process variables on stainless steel grade SS 316L, manufactured through the laser-powder bed fusion process (L-PBF), during high-speed turning. The analysis includes cutting speed, depth of cut, and feed rate. Parametric optimization was performed to achieve the desired response characteristics, reducing machining cost, carbon emissions, specific energy, tool life, and surface roughness. Popović et al. [16] investigated optimal parameters for PLA polymer FDM parts, focusing on nozzle temperature and printing speed. Results show that 190°C and 40 mm/min are most effective, but 80 mm/min speed may be considered for higher FDM productivity. Harris et al. [17] explored the impact of volume distributions (10–90%) on the tensile, flexure, and compressive characterization of FFF and epoxy systems. It uses scanning electron microscopy (SEM) and a high-quality camera for mechanical characterization. The study reveals high tensile strain and compressive strength for lower FDM percentages, suggesting potential for future material-based innovations in HDM. Abbas et al. [18] examined the effects of FDM parameters (outer shell width, infill density, layer thickness, and infill pattern) on PLA compressive properties, revealing that while layer thickness has a minor impact on compressive resistance, infill density plays a more significant role. Abas et al. [19] examined the impact of 3D printing parameters on dimensional deviations in polylactic acid-printed parts. The study found that infill density significantly affects length and width deviation, while layer height significantly affects angle and height deviation. The optimal results were obtained using an integrated approach of desirability and WASPAS, providing a guideline for fabricating assistive devices with high-dimensional accuracy. Kumar et al. [20] conducted an experimental investigation of the influence of FDM parameters (raster width, infill density, and raster angle) on the mechanical characteristics of PLA parts under compressive and flexural loading, observing the considerable impact of infill density on compressive strength and modulus. Begum et al. [21] developed a novel structure for evaluating flexible porosity in bone scaffolds made of polyamide (PA 2200). A CAD model was created using specific input parameters, and the porosity was controlled by varying input parameters. The model showed 29% to 30% reductions in experimental porosity compared to theoretical. Structural analysis and computational fluid dynamics analysis confirmed the model's potential for successful bone implant applications, with a maximum pressure of 1.799 Pa. Abbas et al. [22] studied the main parameters influencing printing time and product weight in the FDM process for ABS thermoplastic products, highlighting the significant impact of infill pattern and density on specimen strength. Ali et al. [23] presented an experimental approach to study the effects of structural factors on the mechanical characteristics of PLA hollow-sphere structures produced with FDM. Parab et al. [24] examined the optimal PLA infill pattern for 3D printing based on compressive strength and found that triangular infill surpassed the default line infill pattern in various test conditions. Syed et al. [25] optimized FDM process parameters for tensile strength, flexural strength, and longitudinal shrinkage using the Grey-Taguchi approach. Input parameters include layer thickness, raster angle, fill density, number of contours, printing temperature, and speed. The Taguchi L27 orthogonal array is used for the statistical design of the experiment, and Grey relational analysis is used for optimization. The optimal parameters minimize longitudinal shrinkage while maximizing tensile and flexural strengths. The qualities of 3D-printed specimens under varied processing circumstances and materials were investigated by Abeykoon et al., [26]. Thermal gravimetric analysis, SEM, differential scanning calorimetry, tensile, compression, bending, and compression testing methods were employed. Young's modulus improved with infill density, according to the results, with pure PLA having the greatest Young's modulus. According to the study, a linear fill pattern, 90°C infill speed, 215°C nozzle temperature, and 100% infill density are the ideal process parameters. Tanga et al. [27] used digital image correlation (DIC) to investigate the mechanical characteristics of 3D-printed PLA lattice constructions. FDM was utilized to create lattice structures and tensile samples. According to the study, tensile strength and elastic modulus increase first and subsequently drop with increasing printing temperature. There is a declining trend in yield strength, densification strain, and plastic platform stress. The rate of printing is likewise increasing. Mauryaa et al. [28] investigated the impact of process variables (infill pattern, layer thickness, build orientation, and infill density) on dimensional accuracy, flatness, and cylindricity in a prototype connecting rod made of polylactic acid, identifying the best parameters for each category.

These studies have collectively played a crucial role in advancing our understanding of the critical parameters influencing the quality and performance of 3D-printed objects using FDM technology. These studies have explored various variables and shed light on their individual and interactive effects on mechanical and physical properties. While these studies have substantially contributed to the field, our work aims to enhance this knowledge base by comprehensively examining the intricate relationships between the selected parameters. The physical and mechanical properties of parts produced with the FDM system vary depending on the specified printing parameters. Some printed samples exhibit poor mechanical and physical properties due to the values of selected printing parameters, which significantly impact the properties of the produced samples. Therefore, this study aims to determine how infill density, infill pattern, overlap percentage, layer thickness, shell thickness, and top/bottom layer number

affect the physical and mechanical properties of printed samples fabricated using the FDM method. Based on test results, the ultimate compression strength (UCS) and average compression deviation percentage of the specimens are evaluated and analyzed to identify variable values that influence the properties of printed specimens.

2. Experimental Work

Polylactic Acid (PLA) material, specifically TORWELL PLA filament, was used to fabricate samples. The samples were produced using a Creality Ender-5 Pro FDM printer equipped with a 0.4 mm diameter nozzle, as depicted in Figure 1. The specifications of the FDM setup are provided in Table 1. PLA, derived from lactic acid building blocks, is known for its biodegradability and bioactivity. It is a versatile, cost-effective material suitable for a wide range of applications and is considered one of the most environmentally friendly fibers currently available, despite its inherent brittleness [29]. Tables 2 and 3 present the specifications and properties of the PLA material, respectively. The specimen was initially designed as a CAD model according to ASTM standard D695, and then converted into STL format for further processing, as shown in Figure 2 (a, b). The workflow of this study is illustrated in Figure 3. Test specimens were designed to investigate the impact of six input factors—infill density, pattern, layer thickness, shell thickness, top/bottom layer number, and infill overlap—across five levels, as outlined in Table 4. Based on the previous research, the most effective parameters in 3D printing research are driven by the need to achieve optimal outcomes in the printed objects: infill density, layer thickness, shell thickness, infill overlap, and top/bottom layer number. The strong point of selecting these parameters lies in their collective influence on critical aspects of the printing process, including strength, surface finish, and dimensional accuracy. By strategically adjusting these parameters, researchers gain comprehensive control over the printing process, allowing for a fine-tuned optimization based on specific objectives. For instance, infill density impacts the internal structure and strength of the object, layer thickness affects resolution and printing speed, shell thickness influences structural integrity, infill overlap determines adhesion between layers, and top/bottom layer number affects surface quality and overall strength.

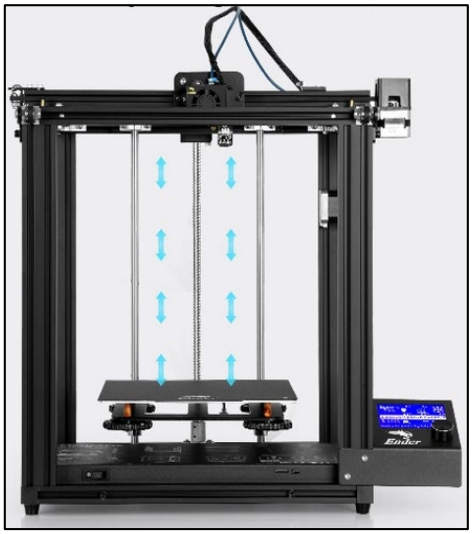

Figure 1: Creality Ender-5 Pro 3D printer

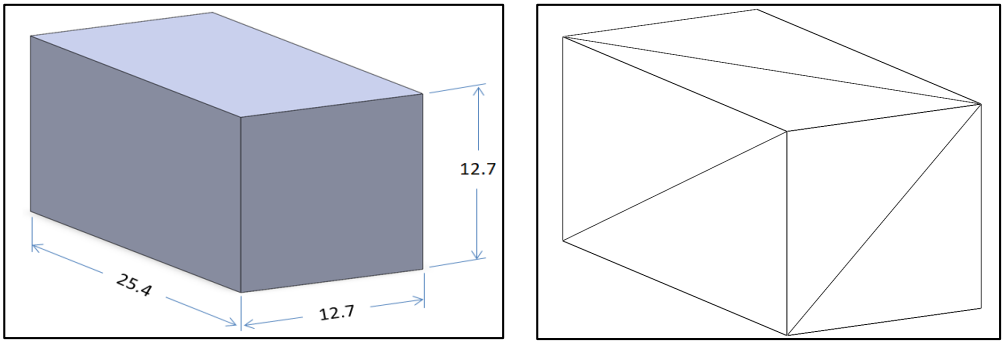

(a) **(b)**

Figure 2: (a) Part SolidWorks Model (all dimensions in mm), (b) SolidWorks Model STL File

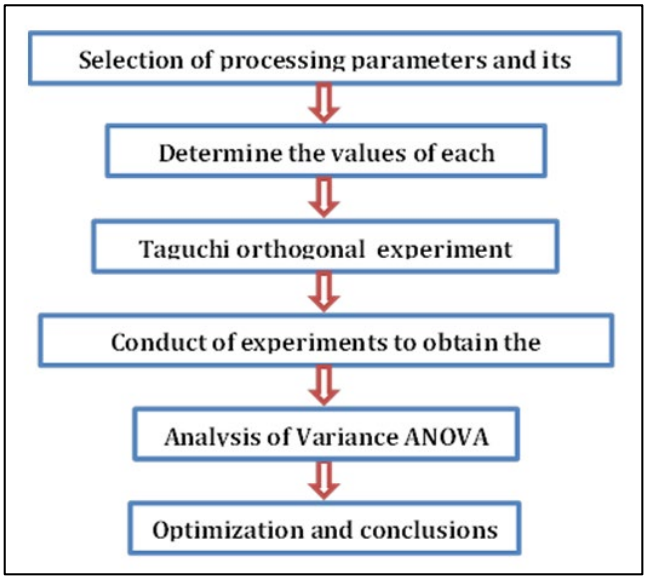

Figure 3: Proposed workflow

Table 1: FDM setup's specifications

No.	Parameters	Values
1	Layer thickness	100 - 400 Microns
2	Precision of print	+/- 100 microns
3	Max extruder temperature	260°C
4	Nozzle size	0.4 mm (0.2 and 0.3 mm supported)
5	Filament type	ABS, TPU, PETG, PLA, Wood
6	Print bed	Heated bed with soft magnetic stickers
7	Max hotbed temperature	135°C
8	Print area	220 x 220 x 300 mm
9	Bed leveling	Manual
10	Display	LCD screen

Table 2: PLA filament specification

Parameter	Unit
Material	PLA with a diameter of 1.75 mm and 330 meters in length
Weight	1 kg for each spool
Melt point	195–235
Density at 21.5	1.25 g/cm^3
Impact strength	12 kJ/m

Table 3: PLA Properties

Property Type	The Value
Flexural strength	48–110 MPa
Tensile strength	61–66 MPa
Fracture elongation	0.7%
Modulus of tensile	2.7–16 Gpa

Table 4: Process parameters of PLA filament

		Levels				
FDM parameters		1	2	3	4	5
	Infill density%	20	40	60	80	100
	Infill pattern	Grid	Triangles	Cubic	Lines	Tri-Hexagon
	Layer thickness	0.10	0.15	0.20	0.25	0.30
	Shell thickness	0.4	0.8	1.2	1.6	2.0
	Top/bottom layer no.	2	3	4	5	6
	Infill overlap%	0	5	10	15	20

An influential, straightforward, and systematic technique is developed by designing experiments using the Taguchi method to identify the ideal machining conditions in the production process. The Taguchi approach was employed to set up the experiment. Six process parameters were examined to understand how FDM parameters affected compression strength: infill density percentage, infill pattern, layer thickness, number of top/bottom layers, shell thickness, and infill overlap percentage.

Each of these parameters had five levels of variation. The Taguchi method evaluated the performance characteristic that deviates from the desired values using the signal-to-noise (S/N) ratio [30–32]. The Taguchi method is favored for determining optimal machining conditions because it emphasizes robust design and efficiency. Its key strengths include focusing on finding conditions less sensitive to variations, using fractional factorial design for efficient study of multiple factors, employing the Signal-to-Noise ratio for comprehensive assessment, utilizing orthogonal arrays for balanced exploration of factor space and is known for cost-effectiveness in industrial settings. To maximize compression strength and minimize compression average deviation percentage, the higher-the-better compression strength and the lower-the-better dimensional accuracy should be selected. Equations 1 and 2 can represent the S/N ratio for the higher-the-better and smaller-the-better performance characteristics, respectively:

1) Larger is bette:

$$S/N = -10\log\left(\frac{1}{n}\sum_{i=1}^{n}\frac{1}{y_i^2}\right) \quad (1)$$

2) Smaller is better:

$$S/N = -10\log\left(\frac{1}{n}\sum_{i=1}^{n}y_i^2\right) \quad (2)$$

where n = total number of measurements, yi = value of the measured characteristics.

At room temperature, the specimens were tested in accordance with ASTM D695 standards on a WDW-200E computer-controlled electronic universal testing machine, as illustrated in Figure 4, with a crosshead speed of 1.5 mm/min to evaluate the mechanical properties of the fabricated specimens. Load, deformation, stroke, and time data were recorded during the experiments. The ultimate compression strength was determined using the recorded data. The stresses and mechanical properties were determined using the actual dimensions of each specimen rather than the CAD model. The compression strength of each PLA test sample was estimated using Equation 3. The various PLA filament test specimens are shown in Figure 5.

$$\sigma = F/A \quad (3)$$

where: σ = Compression stress (N/mm²), F = Applied force (N), A = Cross-sectional area of the fabricated part (mm²)

Figure 4: WDW-200E computer-controlled electronic universal testing machine

Figure 5: PLA filament testing specimens after the test

All the molded specimens were compared to the CAD model to assess the influence of the processing parameters on the compression average percentage deviation (dimensional accuracy). Digital vernier calipers were used to measure each specimen's dimensions. For each run, every piece of geometry was measured three times. The average percentage deviation for the geometry was then determined using Equations (3-5) [33].

$$\text{Deviation } (D_i) = |\text{Specified Dimension} - \text{Observed Value}| \quad (3)$$

$$\text{Percentage Deviation } (D_{pi}) = \left(\frac{\text{Deviation (Di)}}{\text{Specified Dimension}}\right) \times 100 \quad (4)$$

$$\text{Average Percentage Deviation} = \frac{D_{p1}+D_{p2}+D_{p3}}{3} \quad (5)$$

3. Results and Discussion

The results in Table 5 illustrate the impact of six printing parameters on the Ultimate Compression Strength (UCS) and compression average percentage deviation (dimensional accuracy) for 25 specimens.

Table 5: Ultimate compression strength (UCS) and compression average percentage deviation of printed parts

NO.	Infill density %	Infill pattern	Layer thickness (mm)	Shell thickness (mm)	Top/Bottom layer No.	Infill overlap %	UCS MPa	Compression Average Percentage Deviation
1	20	Grid	0.10	0.4	2	0	4.050	1.02367
2	20	Triangles	0.15	0.8	3	5	9.879	1.10267
3	20	Cubic	0.20	1.2	4	10	18.957	1.12867
4	20	Lines	0.25	1.6	5	15	23.849	0.78733
5	20	Tri-Hexagon	0.30	2.0	6	20	33.148	1.28600
6	40	Grid	0.15	1.2	5	20	20.441	0.76100
7	40	Triangles	0.20	1.6	6	0	27.760	0.70867
8	40	Cubic	0.25	2.0	2	5	29.235	0.91867
9	40	Lines	0.30	0.4	3	10	13.585	0.81367
10	40	Tri-Hexagon	0.10	0.8	4	15	20.277	0.65600
11	60	Grid	0.20	2.0	3	15	38.128	0.81367
12	60	Triangles	0.25	0.4	4	20	26.992	0.84000
13	60	Cubic	0.30	0.8	5	0	31.161	1.65367
14	60	Lines	0.10	1.2	6	5	28.185	0.86600
15	60	Tri-Hexagon	0.15	1.6	2	10	30.095	0.49900
16	80	Grid	0.25	0.8	6	10	38.541	0.89233
17	80	Triangles	0.30	1.2	2	15	36.726	1.28633
18	80	Cubic	0.10	1.6	3	20	46.116	0.73500
19	80	Lines	0.15	2.0	4	0	44.500	0.57733
20	80	Tri-Hexagon	0.20	0.4	5	5	36.806	0.99733
21	100	Grid	0.30	1.6	4	5	55.379	1.20700
22	100	Triangles	0.10	2.0	5	10	56.441	0.52467
23	100	Cubic	0.15	0.4	6	15	55.755	0.44633
24	100	Lines	0.20	0.8	2	20	56.469	0.62967
25	100	Tri-Hexagon	0.25	1.2	3	0	49.643	1.31200

4. Results From The Compression Test

The Ultimate Compression Strengths (UCS) of the specimens are presented in Table 5. Figure 6 displays the main-effects graph for the response parameter, i.e., the compression strength of FDM parts. According to Figure 6, this study explored the influence of FDM parameters on the ultimate compression strengths of the specimens. As evident from the trend lines, infill density is the most significant parameter affecting compression strength. Higher infill density means more material inside the part, providing better support and reinforcement to the part's interior, thus making it more resistant to compressive forces. The experimental results presented in this study demonstrate that increasing infill density leads to higher compression strength. For instance, a specimen with 100% infill density exhibits a compression strength of 56.5 MPa, approximately ten times higher than that of a specimen with 20% infill density (4 MPa). However, it's worth noting that the expected maximum compressive strength based on reference [34] is 44.64 MPa for the specimen, whereas the strength at 100% is equal to the 65.9 MPa claimed in literature [17]. The increase in infill density is associated with increased material usage. While maximum strength can be achieved with 100% infill density, it's important to consider cost, printing time, and material consumption when determining the necessary infill density based on the product's type and application. In addition, as seen in Figure 7, the line infill pattern outperforms other patterns by providing a maximum compression strength of 56.5 MPa among the five chosen patterns. This superiority can be attributed to the line infill pattern's ability to evenly distribute loads during compression, reducing voids or areas with less material that could weaken the structure. Additionally, the line pattern aligns with the primary stress direction, enhancing resistance to compression forces in that specific direction. A layer thickness of 0.2 mm yields the best compression strength. This may be because a thinner layer allows for more controlled extrusion, providing the filament with adequate melting time. Conversely, compared to a 0.1 mm layer thickness, a 0.2 mm layer thickness has fewer layers, reducing the risk of inter-layer failure and improving overall mechanical properties. Figure 6 shows that a 2 mm shell thickness results in the highest UCS value among shell thickness variations. Similarly, specimens with 6 top/bottom layers and 20% infill overlap exhibit the highest UCS values. Conversely, specimens with a 0.4 mm shell thickness generally demonstrate lower UCS values. The UCS shows a linear increase with more top/bottom layers.

An analysis of variance (ANOVA) was performed to determine the parameter significance of output responses. The impact of the parameters was compared across all parameter levels and experiment repeats. The p-value is evaluated in comparison to the $\alpha = 0.05$ confidence interval. By showing a 95% confidence interval, the α aids in interpreting the parametric significance. The process parameter with a low p-value relative to α is classified as a significant variable in the response. In addition, all input control parameters are compared, and the significance is evaluated using the previously stated criteria [35–37]. The Taguchi L25 orthogonal array and the signal-to-noise (SN) ratio of leading and trailing observations of compression strength and average percentage deviation have been calculated. Table 6 presents the ANOVA test results for compression strength. Analysis of Variance (ANOVA) was employed to assess the P-value and identify the printing parameter with the most significant impact on compression strength. The compression strength results were obtained, and Table 6 displays the percentage contribution of each parameter along with individual P-values and F-values. From the P-values in the ANOVA table, it can be deduced that infill density % and shell thickness are the most significant parameters affecting compression strength, with a P-value of 0.000 at a 95% confidence level. Infill density refers to the quantity of material utilized to fill the interior space of a 3D-printed object, and higher infill densities typically result in stronger parts due to the increased material content needed to withstand compressive forces. Similarly, a thicker shell provides better resistance to compression forces by creating a more robust exterior structure. In contrast, infill overlap % with a P-value of 0.052, infill pattern with a P-value of 0.218, and layer thickness with a P-value of 0.285 do not show significant influence. In addition to the p-value, which determines the significance of the parameter, the influence of the analyzed parameters can also be estimated based on the percentage contribution of each parameter to the total variation of the experimental results [38- 40]. This analysis confirms that the percentage of infill density has the greatest influence on compression strength, contributing 78.856% at a 95% confidence level, as shown in Figure 8.

Table 6: Results of Analysis of Variance Tests for Compression Strength

Source	DF	Adj SS	Adj MS	F-Value	P-Value	Contribution%	Significance
Infill density %	1	4111.35	4111.35	275.55	0.000	78.856	Yes
Layer thickness	1	18.35	18.35	1.23	0.285	0.352	No
Shell thickness	1	532.22	532.22	35.67	0.000	10.208	Yes
Top/bottom layer no.	1	164.25	164.25	11.01	0.005	3.150	No
Infill overlap %	1	66.48	66.48	4.46	0.052	1.275	No
Infill pattern	4	97.30	24.33	1.63	0.218	1.866	No
Error	15	223.81	14.92			4.293	
Total	24	5213.76				100	

Df = Degrees of freedom; SS = Sum of squares; MS = Mean squares.

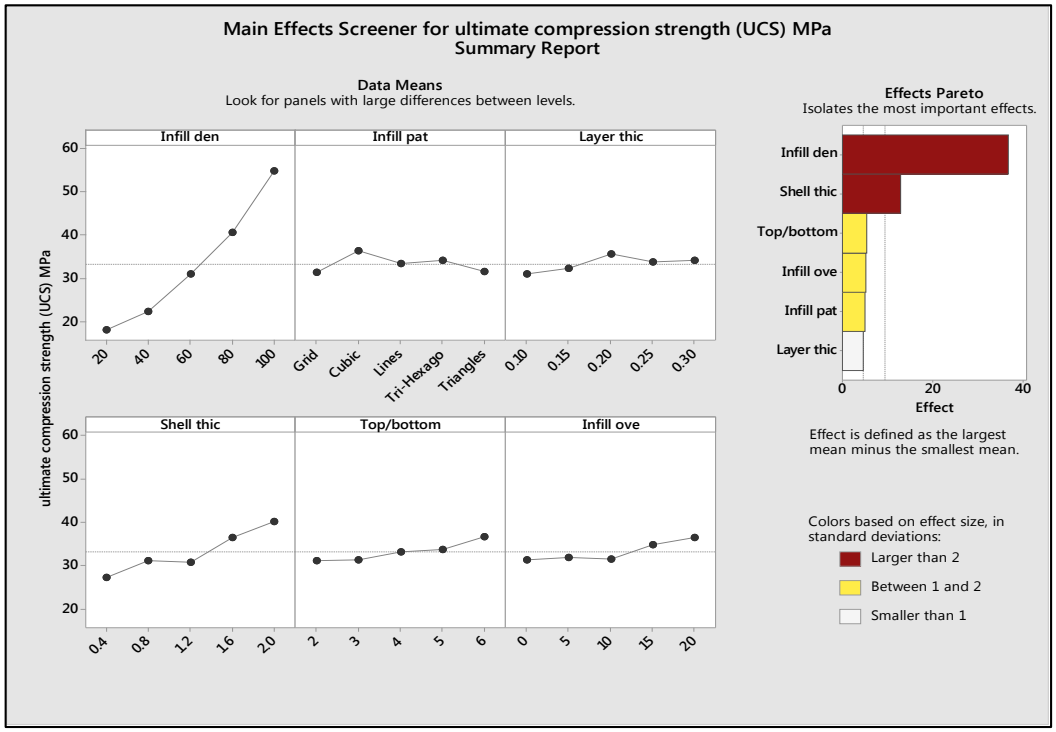

Figure 6: Main effect plot for ultimate compression strength (UCS) MPa

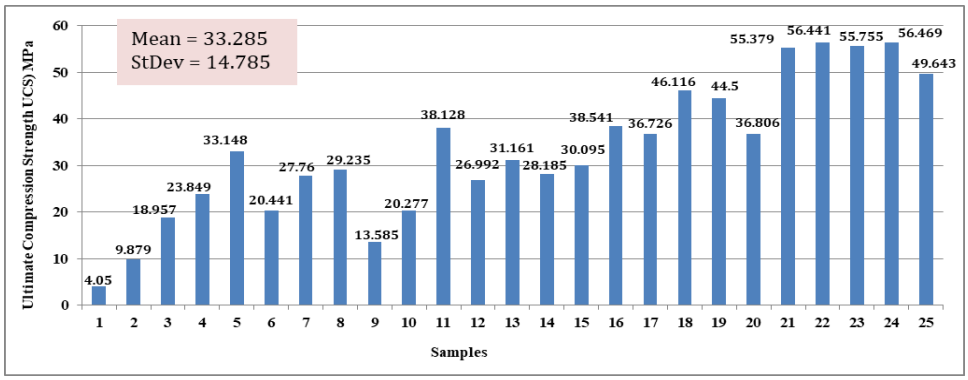

Figure 7: Ultimate compression strength (UCS) variation with FDM parameters for printed parts

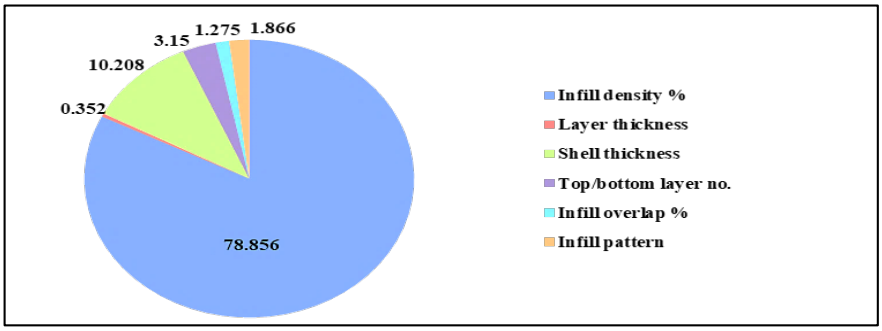

Figure 8: Process parameters contributions of compressive strength

5. Results of Compression Average Percentage Deviation

On the other hand, the compression average percentage deviation of the specimens is presented in Table 5. Figure 9 illustrates the main-effects graph for the response parameter, namely, the compression average percentage deviation of FDM parts. As shown in Figure 9, this study investigated the impact of FDM parameters on the compression average percentage deviation of the specimens. As evident from the trend lines, layer thickness is the most influential parameter affecting the compression average percentage deviation. Layer thickness directly impacts the vertical resolution of a 3D print. A smaller layer thickness results in finer layers, enabling a more accurate representation of intricate details and curved surfaces. Conversely, thicker layers may lead to a loss of detail and a less accurate representation of the original design.

As demonstrated, the specimen with a 0.15mm layer thickness exhibited the minimum deviation in dimensional accuracy for 3D printed parts (0.44633%), approximately three times less than that of the specimen with a 0.3 mm layer thickness

(1.65367%). However, it's worth noting that the expected minimum percentage deviation based on reference [33] is 2.8%, while the expected maximum value is 9.07% for specimens. Thinner layers can promote better adhesion and bonding between successive layers, which can help prevent delamination or warping, ultimately enhancing dimensional accuracy. The increase in layer thickness has been associated with an increase in the deviation observed in PLA parts. A similar study [28] on PLA parts reported a smaller deviation in dimensional accuracy at 100 µm layer thickness. Additionally, as shown in Figure 10, the cubic pattern resulted in a minimum deviation of (0.446%) among the five selected infill patterns. This can be attributed to the cubic infill pattern's composition of evenly spaced, interlocking cubes, providing a highly uniform and stable internal structure. This uniformity improves dimensional accuracy by reducing the likelihood of warping, distortion, or inconsistent layer adhesion. Unlike some infill patterns that may have larger voids or open spaces, the cubic pattern densely fills the interior of the part. Fewer voids mean less potential for structural deformation or deviation from the intended dimensions. The cubic pattern's regular and predictable geometric layout makes it easier to anticipate how the infill will interact with the shell of the part during printing, minimizing the chances of unexpected dimensional variations.

The Taguchi L25 orthogonal array and the signal-to-noise (SN) ratio of leading and trailing observations of compression strength and average percentage deviation have been computed. Table 7 presents the ANOVA test results for the compression average percentage deviation. It can be inferred from the P-values in the ANOVA table that layer thickness is the most significant parameter affecting compression average percentage deviation (dimensional accuracy), with a P-value of 0.002 at the 95% confidence level. Layer thickness plays a pivotal role because it directly impacts the resolution and precision of the printed object. Thinner layers lead to finer details and smoother surfaces, thus enhancing overall dimensional accuracy. The influence of the analyzed parameters can also be estimated by considering the percentage contribution of each parameter to the total variation in the experimental results. This analysis confirms that the percentage of layer thickness exerts the greatest influence on compression average percentage deviation, contributing 37.013% at the 95% confidence level, as depicted in Figure 11.

Table 7: Results of Analysis of Variance Tests for Compression Average percentage deviation

Source	DF	Adj SS	Adj MS	F-Value	P-Value	Contribution %	Significance
Infill density %	1	0.06387	0.063867	1.12	0.307	3.0292	No
Layer thickness	1	0.78042	0.780417	13.66	0.002	37.013	Yes
Shell thickness	1	0.01995	0.019947	0.35	0.563	0.946	No
Top/bottom layer no.	1	0.00272	0.002723	0.05	0.830	0.129	No
Infill overlap %	1	0.19837	0.198366	3.47	0.082	9.408	No
Infill pattern	4	0.18628	0.046570	0.82	0.535	8.835	No
Error	15	0.85688	0.057125			40.64	
Total	24	2.10848				100	

Df = Degrees of freedom; SS = Sum of squares; MS = Mean squares.

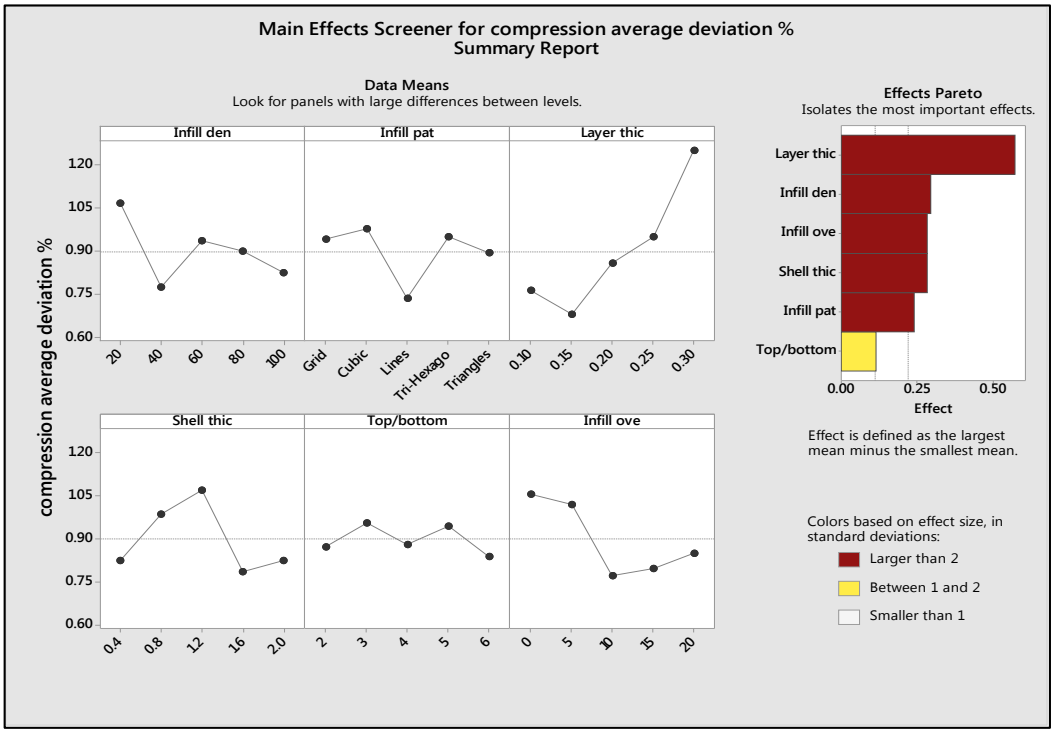

Figure 9: Main effect plot for compression average percentage deviation

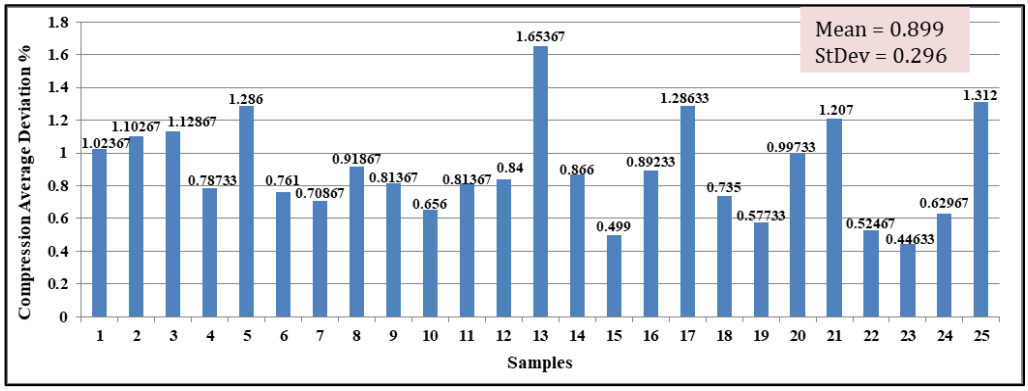

Figure 10: Compression average percentage deviation variation with FDM parameters for printed parts

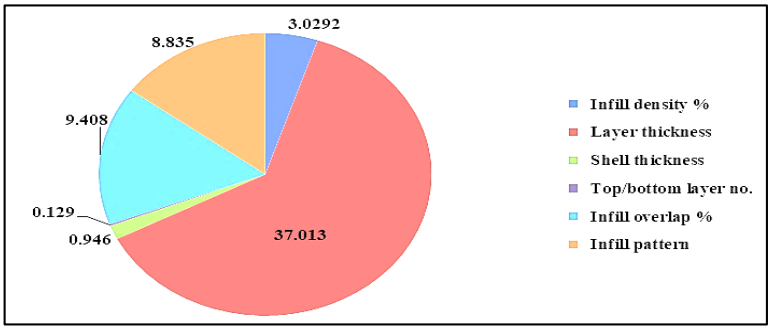

Figure 11: Process parameters contributions of compressive average percentage deviation

Surface topography is crucial for understanding the quality of the printed surface. Therefore, critical experimental observations were conducted using a Stereo microscope, and these results are presented in Figure 12. Figure (12-a) depicts that specimens formed with 100% infill density, a line pattern, 0.2mm layer thickness, 0.8mm shell thickness, 2 top/bottom layer numbers, and 20% overlap exhibit rough fractured surfaces. These specimens feature material failure during compressive loading, resulting in higher compressive strength. In contrast, Figure (12-b) illustrates specimens that ruptured along the layers, forming smooth fractured surfaces. This suggests that specimens with 20% infill density, a grid pattern, 0.1mm layer thickness, 0.4 mm shell thickness, 2 top/bottom layer numbers, and 0% overlap did not allow the material to resist the compressive load effectively. The failure occurred due to poor interfacial adhesion between the layers, leading to lower compressive strength. The specimens formed with these parameters were ineffective in transferring compressive load from one layer to another, resulting in lower strength. On the other hand, Figure (12-c) demonstrates minimal deviation in dimensional accuracy, achieved with a low layer thickness and a higher top/bottom layer number. This is attributed to the direct impact of layer thickness on vertical resolution, while the top/bottom layer number influences the surface quality of a 3D print. In contrast, Figure (12-d) illustrates a higher deviation in dimensional accuracy.

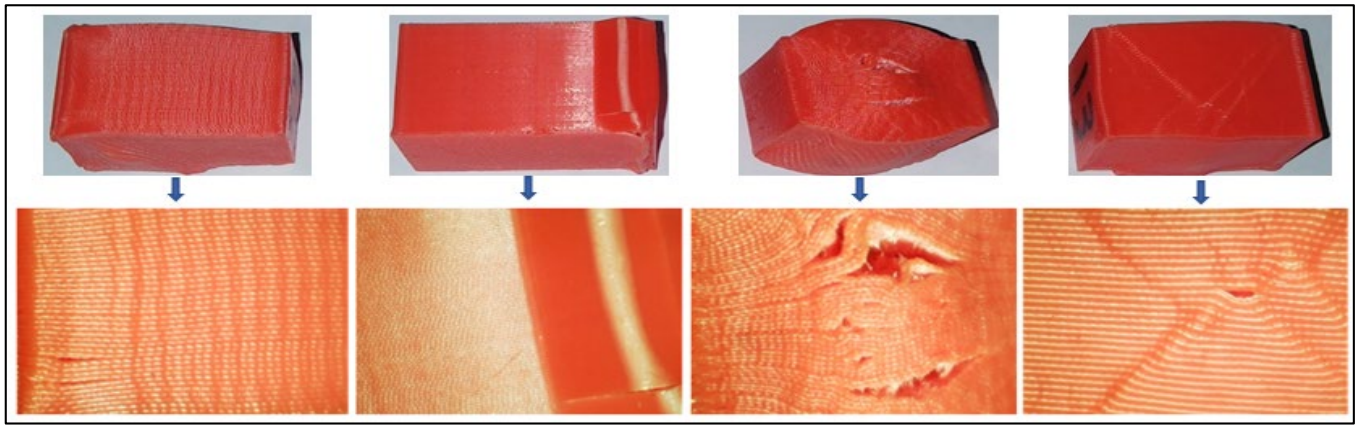

Figure 12: Surface topography of fractured samples using Stereo Scope (20x magnification) for (a) maximum ultimate compression strength UCS MPa, (b) minimum ultimate compression strength UCS MPa, (c) minimum average compression percentage deviation, and (d) maximum average compression percentage deviation

The changes in mechanical and physical properties of test specimens fabricated using different process parameters are illustrated in the interaction graphs in Figures 13 and 14. These interaction plots demonstrate how the value of the second categorical parameter influences the relationship between one categorical parameter and a continuous response. On the x-axis of these plots are the means for the levels of one parameter, and separate lines are shown for each level of another parameter.

Notably, the lines in these interaction plots are not parallel, indicating that the value of FDM parameters has a discernible impact on both compression strength and dimensional accuracy. Figure 13 illustrates that the strength levels are notably higher for a line infill pattern with 100% infill density, a layer thickness of 0.2 mm, a shell thickness of 0.8 mm, 2 top and bottom layers, and a 20% infill overlap. Figure 14 shows that the minimum average compression deviation percentage occurs with 100% infill density, a cubic pattern, a layer thickness of 0.15 mm, a shell thickness of 0.4 mm, 6 top and bottom layers, and a 15% infill overlap.

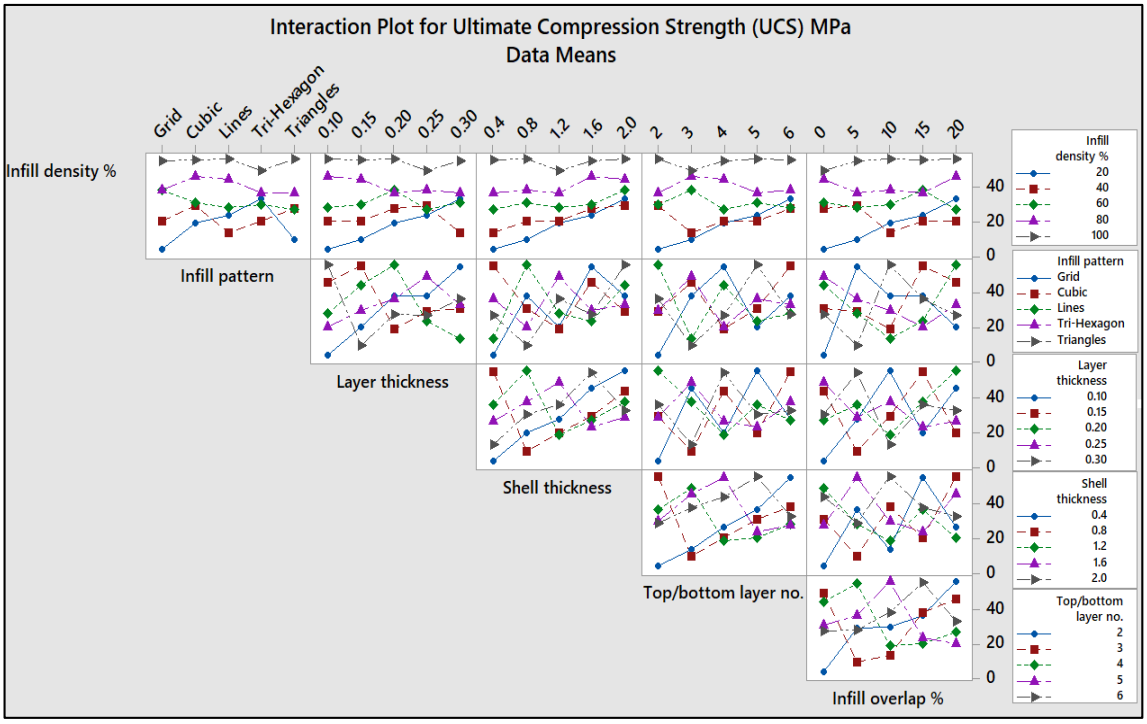

Figure 13: Plot for compression strength interaction

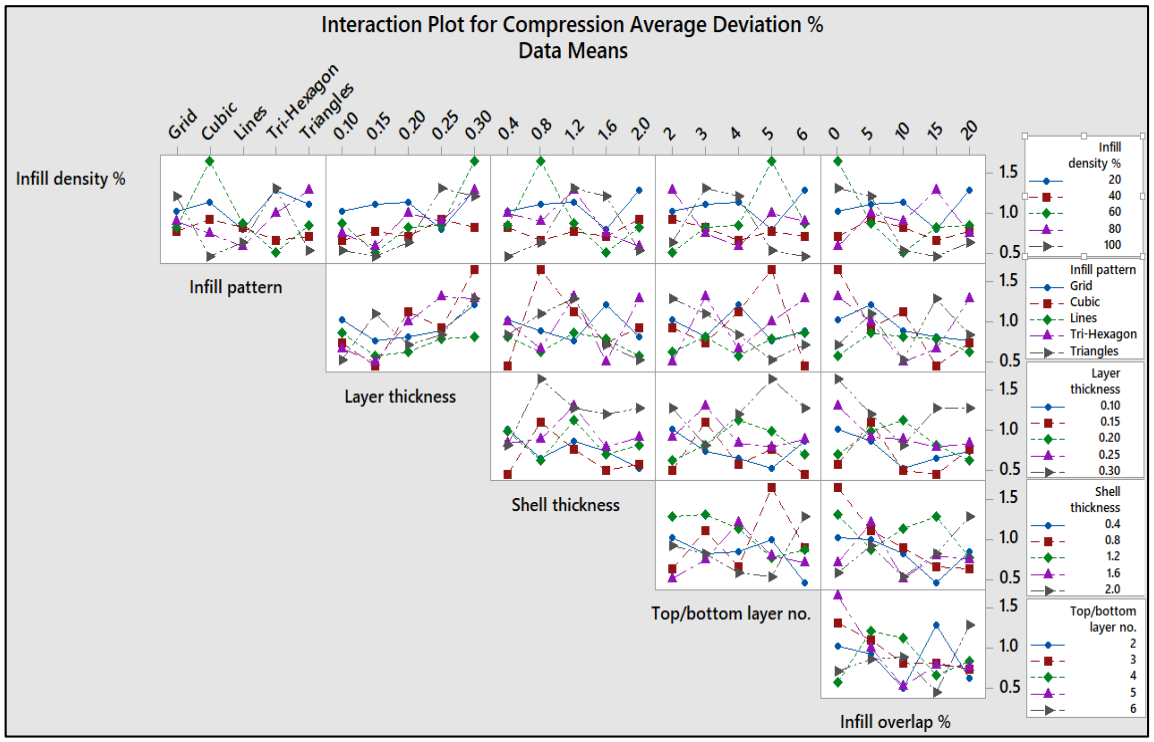

Figure 14: Plot for compression average percentage deviation interaction

Cubic mathematical models were formulated based on the experimental results listed in Table 5, using Minitab 17 and employing regression analysis. This process involved fitting a model to the experimental data to establish a functional relationship between FDM parameters and response properties. Equations 7–11, presented in Appendix A, represent the mathematical models for the relationship between infill pattern and compression strength. Considering various process parameters, they serve as a valuable tool for predicting compression strength in our 3D printing process. Conversely, Equations 12–16, as illustrated in Appendix A, depict the mathematical models for the relationship between infill pattern and compression

average percentage deviation, which is a valuable tool for predicting minimum deviation in dimensional accuracy while considering the same process parameters.

The percentage error between the measured and predicted ultimate compression strength (UCS) and compression average percentage deviation of PLA parts was calculated according to Equation 6. Table 8 presents the results, showing that the maximum percentage error values between the measured and predicted Ultimate Compression Strength (UCS) and compression average deviation% of PLA parts were 0.44% and 0.948%, respectively. Conversely, the minimum percentage error values between the measured and predicted Ultimate Compression Strength (UCS) and compression average deviation of PLA parts were 0.10% and 0.041%, respectively, as depicted in Figures 15 and 16. These percentage error results are deemed acceptable, indicating that the model has performed satisfactorily predicting the responses.

$$\text{Error } \% = |((\text{measured UCS} - \text{Predicted UCS}) / \text{measured UCS}) \times 100| \quad (6)$$

Table 8: Percentage error for ultimate compression strength (UCS) of PLA parts

NO.	Measured UCS (MPa)	Predicted UCS (MPa)	Error %	Measured Compression Average Percentage Deviation	Predicted Compression Average Percentage Deviation	Error %
1	4.050	4.0616	0.29	1.0237	1.0227	0.095
2	9.879	9.8559	0.23	1.1027	1.1014	0.115
3	18.957	18.8866	0.37	1.1287	1.1267	0.175
4	23.849	23.7538	0.40	0.7873	0.7859	0.182
5	33.148	33.0274	0.36	1.2860	1.2840	0.156
6	20.441	20.3789	0.30	0.7610	0.7591	0.250
7	27.760	27.6947	0.24	0.7087	0.7054	0.461
8	29.235	29.1779	0.20	0.9187	0.9159	0.302
9	13.585	13.5251	0.44	0.8137	0.8127	0.119
10	20.277	20.2087	0.34	0.6560	0.6544	0.244
11	38.128	38.0865	0.11	0.8137	0.8127	0.119
12	26.992	26.9239	0.25	0.8400	0.8380	0.238
13	31.161	31.0807	0.26	1.6537	1.6502	0.210
14	28.185	28.0841	0.36	0.8660	0.8631	0.335
15	30.095	30.0403	0.18	0.4990	0.4981	0.180
16	38.541	38.4697	0.18	0.8923	0.8886	0.418
17	36.726	36.6755	0.14	1.2863	1.2858	0.041
18	46.116	46.0135	0.22	0.7350	0.7310	0.544
19	44.500	44.4089	0.20	0.5773	0.5746	0.473
20	36.806	36.7255	0.22	0.9973	0.9942	0.314
21	55.379	55.3223	0.10	1.2070	1.2045	0.207
22	56.441	56.3300	0.20	0.5247	0.5216	0.585
23	55.755	55.6227	0.24	0.4463	0.4421	0.948
24	56.469	56.3825	0.15	0.6297	0.6304	0.116
25	49.643	49.5690	0.15	1.3120	1.3098	0.168

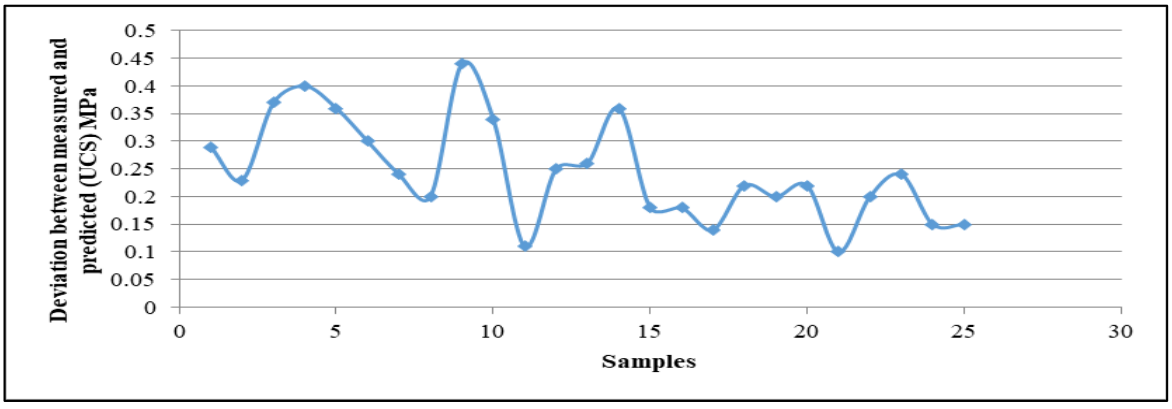

Figure 15: Relationship between error (percentage error between measured and predicted (UCS) MPa) and number of experiments

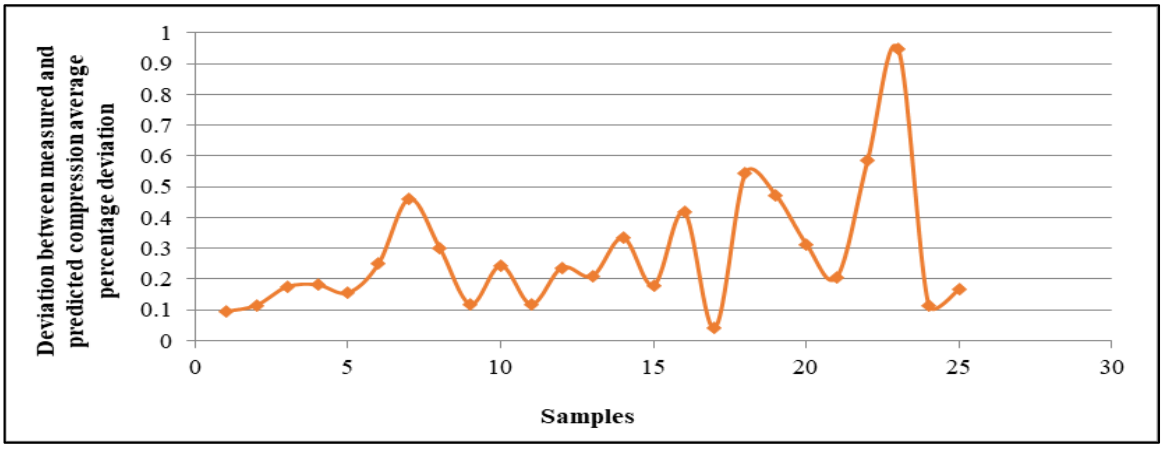

Figure 16: Relationship between error (percentage error between measured and predicted compression average percentage deviation) and number of experiments

6. Conclusion

The impact of FDM parameters on the compression test mechanical characteristics and dimensional accuracy of FDM specimens was investigated using Taguchi's L25 DOE. Before compression testing, linear dimension measurements were performed to assess the specimens' dimensional accuracy, following the ASTM D695 standard. Based on the experimental results, the following conclusions could be drawn:

1) Based on the findings regarding the mechanical characteristics of the fabricated specimens, it was determined that a combination of parameters, including 100% infill density, a line infill pattern, 0.2 mm layer thickness, 0.8 mm shell thickness, two top and bottom layers, and 20% infill overlap optimized the compression strength of parts, achieving a value of 56.5 MPa.
2) Regarding the physical characteristics of the FDM specimens, it was found that a cubic pattern with 100% infill density, 0.15 mm layer thickness, 0.4 mm shell thickness, 6 top/bottom layers, and 15% infill overlap exhibited the lowest average percentage deviation among the selected parameters, with a value of 0.446%.
3) The ANOVA analysis concluded that infill density had the most significant impact on compression strength, contributing 78.856%. On the other hand, layer thickness had the greatest impact on compression average percentage deviation, with a contribution of 37.013%.
4) A comparison between the predicted and measured results has been recorded, and the maximum percentage error of the model that fits the data well was 0.44% and 0.948% for ultimate compression strength (UCS) and compression average percentage deviation, respectively.
5) In conclusion, it is evident that optimizing mechanical and physical properties simultaneously through FDM parameter selection is challenging. To enhance the strength of printed parts, it is recommended to use a line infill pattern, 100% infill density, 0.2 mm layer thickness, 0.8 mm shell thickness, two top and bottom layers, and 20% infill overlap as FDM parameters. Conversely, to minimize dimensional accuracy deviation, choosing a cubic infill pattern, 100% infill density, 0.15 mm layer thickness, 0.4 mm shell thickness, 6 top/bottom layer numbers, and 15% infill overlap as FDM parameters is advisable. Consequently, optimizing one property may come at the expense of the other, necessitating trade-offs or multi-objective optimization

Appendix A: Predicted Mathematical Model for both Ultimate Compression Strength UCS and compression average percentage deviation

Grid

$$UCS = 104.3 - 1.068\,a - 290.2\,b - 5.480\,c - 45.90\,d + 7.579\,e + 7.001\,ab - 0.5595\,ac + 0.4868\,ad - 0.003433\,ae + 16.21\,bc + 4.943\,bd + 1.203\,be + 18.83\,cd + 1.405\,ce - 1.186\,de - 1.777\,abc - 0.01253\,abd - 0.1649\,abe - 0.005857\,acd - 0.02803\,ace \quad (7)$$

Cubic

$$UCS = 112.4 - 1.068\,a - 290.2\,b - 5.480\,c - 45.90\,d + 7.579\,e + 7.001\,ab - 0.5595\,ac + 0.4868\,ad - 0.003433\,ae + 16.21\,bc + 4.943\,bd + 1.203\,be + 18.83\,cd + 1.405\,ce - 1.186\,de - 1.777\,abc - 0.01253\,abd - 0.1649\,abe - 0.005857\,acd - 0.02803\,ace \quad (8)$$

Lines

$$UCS = 106.2 - 1.068\,a - 290.2\,b - 5.480\,c - 45.90\,d + 7.579\,e + 7.001\,ab - 0.5595\,ac + 0.4868\,ad - 0.003433\,ae + 16.21\,bc + 4.943\,bd + 1.203\,be + 18.83\,cd + 1.405\,ce - 1.186\,de - 1.777\,abc - 0.01253\,abd - 0.1649\,abe - 0.005857\,acd - 0.02803\,ace \quad (9)$$

Tri-Hexagon

$$UCS = 99.27 - 1.068\,a - 290.2\,b - 5.480\,c - 45.90\,d + 7.579\,e + 7.001\,ab - 0.5595\,ac + 0.4868\,ad - 0.003433\,ae + 16.21\,bc + 4.943\,bd + 1.203\,be + 18.83\,cd + 1.405\,ce - 1.186\,de - 1.777\,abc - 0.01253\,abd - 0.1649\,abe - 0.005857\,acd - 0.02803\,ace \quad (10)$$

Triangle

$$UCS = 109.3 - 1.068\,a - 290.2\,b - 5.480\,c - 45.90\,d + 7.579\,e + 7.001\,ab - 0.5595\,ac + 0.4868\,ad - 0.003433\,ae + 16.21\,bc + 4.943\,bd + 1.203\,be + 18.83\,cd + 1.405\,ce - 1.186\,de - 1.777\,abc - 0.01253\,abd - 0.1649\,abe - 0.005857\,acd - 0.02803\,ace \quad (11)$$

Grid

$$\text{Compression Average Deviation \%} = -0.5832 - 0.02706a + 6.565b - 2.654c + 1.781d - 0.2547e + 0.06699ab + 0.05114ac - 0.01685ad + 0.004320ae + 7.255bc - 5.349bd + 0.5083be - 0.3183cd + 0.1993ce - 0.01356de - 0.1346abc + 0.05887abd - 0.008954abe + 0.001724acd - 0.002710ace \quad (12)$$

Cubic

$$\text{Compression Average Deviation \%} = -0.3009 - 0.02706a + 6.565b - 2.654c + 1.781d - 0.2547e + 0.06699ab + 0.05114ac - 0.01685ad + 0.004320ae + 7.255bc - 5.349bd + 0.5083be - 0.3183cd + 0.1993ce - 0.01356de - 0.1346abc + 0.05887abd - 0.008954abe + 0.001724acd - 0.002710ace \quad (13)$$

Lines

$$\text{Compression Average Deviation \%} = -0.7751 - 0.02706a + 6.565b - 2.654c + 1.781d - 0.2547e + 0.06699ab + 0.05114ac - 0.01685ad + 0.004320ae + 7.255bc - 5.349bd + 0.5083be - 0.3183cd + 0.1993ce - 0.01356de - 0.1346abc + 0.05887abd - 0.008954abe + 0.001724acd - 0.002710ace \quad (14)$$

Tri-Hexagon

$$\text{Compression Average Deviation \%} = -0.5570 - 0.02706a + 6.565b - 2.654c + 1.781d - 0.2547e + 0.06699ab + 0.05114ac - 0.01685ad + 0.004320ae + 7.255bc - 5.349bd + 0.5083be - 0.3183cd + 0.1993ce - 0.01356de - 0.1346abc + 0.05887abd - 0.008954abe + 0.001724acd - 0.002710ace \quad (15)$$

Triangles

$$\text{Compression Average Deviation \%} = -0.3417 - 0.02706a + 6.565b - 2.654c + 1.781d - 0.2547e + 0.06699ab + 0.05114ac - 0.01685ad + 0.004320ae + 7.255bc - 5.349bd + 0.5083be - 0.3183cd + 0.1993ce - 0.01356de - 0.1346abc + 0.05887abd - 0.008954abe + 0.001724acd - 0.002710ace \quad (16)$$

where: a : infill density %, b : layer thickness, c : shell thickness, d : top/bottom layer number, e : infill overlap %

Acknowledgment

The experiments were conducted at the Department of Production Engineering and Metallurgy, University of Technology, Baghdad, Iraq.

Author contributions

Conceptualization, H. Abdulridha and T. Abbas; methodology, H. Abdulridha and T. Abbas; software, H. Abdulridha and T. Abbas; validation, H. Abdulridha and T. Abbas; formal analysis, H. Abdulridha and T. Abbas; investigation, H. Abdulridha and T. Abbas; data curation, H. Abdulridha and T. Abbas; writing—original draft preparation, H. Abdulridha and T. Abbas; writing—review and editing, H. Abdulridha and T. Abbas. All authors have read and agreed to the published version of the manuscript.

Funding

This research received no specific grant from any funding agency in the public, commercial, or not-for-profit sectors.

Data availability statement

The data that support the findings of this study are available on request from the corresponding author.

Conflicts of interest

The authors declare that there is no conflict of interest.

References

[1] S S. Fafenrot, N. Grimmelsmann, M. Wortmann, and A. Ehrmann, Three-dimensional (3D) printing of polymer-metal hybrid materials by fused deposition modeling, Materials, 10 (2017) 1199. https://doi.org/10.3390/ma10101199

[2] S. M. Ahmad and S. Y. Ezdeen, Effect of coating on the specific properties and damping loss factor of ultem 1010, Zanco J. Pure Appl. Sci., 33 (2021) 105–116. http://dx.doi.org/10.21271/zjpas

[3] T. F. Abbas, F. M. Othman, and H. B. Ali, Effect of infill Parameter on compression property in FDM Process, Dimensions, 12 (2017) 24–25.

[4] F. A. Naser and M. T. Rashid, The Influence of Concave Pectoral Fin Morphology in the Performance of Labriform Swimming Robot, Iraqi J. Electr. Electron. Eng., 16 (2020) 54–61. https://doi.org/10.37917/ijeee.16.1.7

[5] N. A. Aldeen, B. A. Sadkhan, and B. Owaid, Hand bone orthosis manufacturing using 3d printing technology, J. Eng. Sustain. Dev., 24 (2020) 451–458. https://doi.org/10.31272/jeasd.conf.1.50

[6] M. Rismalia, S. C. Hidajat, I. G. R. Permana, B. Hadisujoto, M. Muslimin, and F. Triawan, Infill pattern and density effects on the tensile properties of 3D printed PLA material, in: Conference Series: J. Physics., 1402 (2019) 44041. https://doi.org/10.1088/1742-6596/1402/4/044041

[7] F. M. Mwema and E. T. Akinlabi, Fused Deposition Modeling: Strategies for Quality Enhancement, Springer Br. Appl. Sci. Technol., 1st ed., 2020.

[8] W. A. Soud, I. A. Baqer and M. aR. Ahmed, Experimental Study of 3D printing Density Effect on the Mechanical Properties of the Carbon-Fiber and Polylactic Acid Specimens, J. Eng. Technol., 37 (2019) 128–132. https://doi.org/10.30684/etj.37.4A.3

[9] F. M. Othman, T. Fadhil, and A. H. B. Ali, Influence of process parameters on mechanical properties and printing time of FDM PLA printed parts using design of experiment, J. Eng. Res., 8 (2018) 2248–9622.

[10] M. L. Dezaki and M. K. A. Mohd Ariffin, The Effects of Combined Infill Patterns on Mechanical Properties in FDM Process, Polymers, 12 (2020) 2792. http://dx.doi.org/10.3390/polym12122792

[11] M. S. Kumar, M. U. Farooq, N. S. Ross, C. H. Yang, V. K. and A. A. Adediran, Achieving effective interlayer bonding of PLA parts during the material extrusion process with enhanced mechanical properties, Scientific Reports, 13 (2023). http://dx.doi.org/10.1038/s41598-023-33510-7

[12] V. V. Ambade, S.W. Rajurkar, G. K. Awari, Effect of Infill Density and Infill Pattern on the Compressive Strength of Parts Printed by PLA Filament using FDM, Int. J. Res. Anal. Rev., 10 (2023).

[13] A. S. Bedan, T. F. Abbas, E. A. Hussein, Prediction and Investigation of the interactive impact of shell thickness and infill density on the mechanical properties and the mass of ABS prints, J. Hunan Univ., (Web of Sciences) 50 (2023). http://dx.doi.org/10.55463/issn.1674-2974.50.1.20

[14] Sivaraos, K. Kumaran, R. Dharsyanth, M. Amran, S. M. Shukor, S. Pujari, D. Ramasamy, U. K. Vatesh, A. S. M. Al-Obaidi, S. Ramesh, K. Y. S. Lee, Predictive Modeling of Dimensional Accuracies in 3d Printing using Artificial Neural Network, J. Eng. Sci. Technol., 18 (2023) 2148 – 2160.

[15] M. U. Farooq, S. Anwar, R. Ullah, R. H. Guerra, Sustainable machining of additive manufactured SS-316L underpinning low carbon manufacturing goal, J. Mater. Res. Technol., 24 (2023) 2299-2318. http://dx.doi.org/10.1016/j.jmrt.2023.03.122

[16] M. Popović, M. Pjević, A. Milovanović, G. Mladenović, M. Milošević, Printing parameter optimization of PLA material concerning geometrical accuracy and tensile properties relative to FDM process productivity, J. Mech. Sci. Technol., 37 (2023) 697–706. http://dx.doi.org/10.1007/s12206-023-0113-6

[17] M. Harris, H. Mohsin, J. Potgieter, K. M. Arif, S. Anwar, A. AlFaify & M. U. Farooq, Hybrid deposition additive manufacturing: novel volume distribution, thermo-mechanical characterization, and image analysis, J. Braz. Soc. Mech. Sci. Eng., 44 (2022). http://dx.doi.org/10.1007/s40430-022-03731-4

[18] T. F. Abbas, K. K. Mansor, H. B. Ali, The Effect of FDM Process Parameters on the Compressive Property of ABS Prints, J. Hunan Univ. Nat. Sci., 49 (2022). http://dx.doi.org/10.55463/issn.1674-2974.49.7.17

[19] M. Abas, T. Habib, S. Noor, B. Salah, and D. Zimon, Parametric Investigation and Optimization to Study the Effect of Process Parameters on the Dimensional Deviation of Fused Deposition Modeling of 3D Printed Parts, Polymers, 14 (2022) 3667. http://dx.doi.org/10.3390/polym14173667

[20] S. Kumar, S. Teraiya, V. K. Koriya, FDM Fabricated PLA Parts: An Experimental Study of Effect of Process Parameters on Mechanical Properties under Compressive and Flexural Loading, Int. J. Mod. Manuf. Technol., 2 (2022) http://dx.doi.org/10.54684/ijmmt.14.2.111

[21] S. R. Begum, M S. Kumar, M Vasumathi, M. U. Farooq, C. I. Pruncu, Revealing the compressive and flow properties of novel bone scaffold structure manufactured by selective laser sintering technique, J. Med. Eng., (2022) 1–13. http://dx.doi.org/10.1177/09544119211070412

[22] T. F. Abbas, H. B. Ali, K. K. Mansor, Influence of FDM Process Variables' on Tensile Strength, Weight, and Actual Printing Time when using ABS Filament, Int. J. Mod. Manuf. Technol., 1 (2022) http://dx.doi.org/10.54684/ijmmt.2022.14.1.7

[23] N. B. Ali, M. Khlif, D. Hammami and C. Bradai, Optimization of structural parameters on hollow spherical cells manufactured by Fused Deposition Modeling (FDM) using Taguchi method, Cellular Polymers, 41 (2022) 3-20. http://dx.doi.org/10.1177/02624893211043324

[24] S. Parab, N. Zaveri, Investigating the Influence of Infill Pattern on the Compressive Strength of Fused Deposition Modelled PLA Parts, in: Proc. Int. Conf. Intell. Manuf. Autom., (2022) 239–247. http://dx.doi.org/10.1007/978-981-15-4485-9_25

[25] M. A. B. Syed, Q. Rhaman, H. M. Shahriar, M. M. A. Khan, Grey-Taguchi Approach for Optimizing Fused Deposition Modeling Process in Terms of Mechanical Properties and Dimensional Accuracy, Int. Conf. Eng. Res. Edu. Sch. Appl. Sci. Technol., SUST, Sylhet, 2021.

[26] C. Abeykoon, P. S. Amphorn, A. Fernando, Optimization of fused deposition modeling parameters for improved PLA and ABS 3D printed structures, Int. J. lightweight mater. manuf., 3 (2020) 284-297. http://dx.doi.org/10.1016/j.ijlmm.2020.03.003

[27] C. Tanga, J.Liua, Y. Yangc, Y. Liua, S. Jianga, W. Hao, Effect of process parameters on mechanical properties of 3D printed PLA lattice structures, Composites Part C: 3 (2020) 100076. http://dx.doi.org/10.1016/j.jcomc.2020.100076

[28] N. K. Mauryaa, V. Rastogib, P. Singh, Fabrication of prototype connecting rod of PLA plastic material using FDM prototype technology, Indian J. Eng. Mater. Sci., 27 (2020) 333-343.

[29] Y. F. Buys, A. N. A. Aznan, and H. Anuar, Mechanical properties, morphology, and hydrolytic degradation behavior of polylactic acid/natural rubber blends, in: IOP Conference Series: Mater. Sci. Eng., 290 (2018) 12077. http://dx.doi.org/10.1088/1757-899X/290/1/012077

[30] K. Ishfaq, M. U. Farooq, C. I. Pruncu, Reducing the geometrical machining errors incurred during die repair and maintenance through electric discharge machining (EDM), Int. J. Adv. Manuf. Technol., 117 (2021) 3153–3168. http://dx.doi.org/10.1007/s00170-021-07846-1

[31] M. U. Farooq, S. Anwar, H. A. Bhatti, M. S. Kumar, M. A. Ali, M. I. Ammarullah, Electric Discharge Machining of Ti6Al4V ELI in Biomedical Industry: Parametric Analysis of Surface Functionalization and Tribological Characterization, Materials, 16 (2023) 4458. http://dx.doi.org/10.3390/ma16124458

[32] M. U. Farooq, S. Anwar, M. S. Kumar, A. AlFaify, M. A. Ali, R. Kumar, R. Haber, A Novel Flushing Mechanism to Minimize Roughness and Dimensional Errors during Wire Electric Discharge Machining of Complex Profiles on Inconel 718, Materials, 15 (2022) 7330. http://dx.doi.org/10.3390/ma15207330

[33] Krishna M. A., Pritish S., Dinesh B., et al, Analyzing the Impact of Print Parameters on Dimensional Variation of ABS specimens printed using Fused Deposition Modelling (FDM), Sensors International, 3 (2022) http://dx.doi.org/10.1016/j.sintl.2021.100149

[34] S. A. Oudah, H. B. Al-Attraqchi, N. A. Nassir, The Effect of Process Parameters on the Compression Property of Acrylonitrile Butadiene Styrene Produced by 3D Printer, J. Eng. Technol., 40 (2022) 189-194. http://dx.doi.org/10.30684/etj.v40i1.2118

[35] M. U. Farooq, M. A. Ali, Y.He, A. M. Khan, C. I. Pruncu, M. Kashif, N. Ahmed, N. Asif, Curved profiles machining of Ti6Al4V alloy through WEDM: investigations on geometrical errors, J. Mater. Res. Technol., 9 (2020) 16186-16201. http://dx.doi.org/10.1016/j.jmrt.2020.11.067

[36] K. Ishfaq, S. Anwar, M. A. Ali, M. H. Raza, M. U.Farooq, S. Ahmad, C. I. Pruncu, M. Saleh, B. Salah, Optimization of WEDM for precise machining of novel developed Al6061-7.5% SiC squeeze-casted composite, J. Manuf. Sci. Technol., 111 (2020) 2031–2049. http://dx.doi.org/10.1007/s00170-020-06218-5

[37] N. Asif, M. Q. Saleem, M. U. Farooq, Performance evaluation of surfactant mixed dielectric and process optimization for electrical discharge machining of titanium alloy Ti6Al4V, CIRP J. Manuf. Sci. Technol., 43 (2023) 42–56. http://dx.doi.org/10.1016/j.cirpj.2023.02.007

[38] K.K.Goyal, N.Sharma, R. D. Gupta, G. Singh, D. Rani, H. K. Banga, R. Kumar, D. Y. Pimenov, K. Giasin, A Soft Computing-Based Analysis of Cutting Rate and Recast Layer Thickness for AZ31 Alloy on WEDM Using RSM-MOPSO, Materials, 15 (2022) 635. http://dx.doi.org/10.3390/ma15020635

[39] M. U. Farooq, M. P. Mughal, N. Ahmed, N. A. Mufti, A. M. Al-Ahmari, Y. He, On the Investigation of Surface Integrity of Ti6Al4V ELI Using Si-Mixed Electric Discharge Machining, Materials, 13 (2020) 1549. http://dx.doi.org/10.3390/ma13071549

[40] M. P.Mughal, M. U. Farooq, J. Mumtaz, M. Mia, M. Shareef, M. Javed, M. Jamil, C. I. Pruncu, journal of the mechanical behavior of biomedical materials 113 (2021) 104145, Surface modification for osseointegration of Ti6Al4V ELI using powder mixed sinking EDM, J. Mech. Behav. Biomed. Mater., 113 (2021) 104145. http://dx.doi.org/10.1016/j.jmbbm.2020.104145